Local control theory for superconducting qubits

M. Mališ,[1] P. Kl. Barkoutsos,[2,3] M. Ganzhorn,[2] S. Filipp,[2] D. J. Egger,[2] S. Bonella,[1] and I. Tavernelli[2,*]

[1]*Centre Européen de Calcul Atomique et Moléculaire, Ecole Polytechnique Fédérale de Lausanne, Avenue Forel 2, 1015 Lausanne, Switzerland*

[2]*IBM Research GmbH, Zurich Research Laboratory, Säumerstrasse 4, 8803 Rüschlikon, Switzerland*

[3]*Institute for Theoretical Physics, ETH Zurich, 8093 Zurich, Switzerland*

(Received 4 September 2018; revised manuscript received 22 February 2019; published 10 May 2019)

In this work, we develop a method to design control pulses for fixed-frequency superconducting qubits coupled via tunable couplers based on local control theory, an approach commonly employed to steer chemical reactions. Local control theory provides an algorithm that only requires a single forward time propagation of the system wave function to shape an external pulse that monotonically increases the population of a desired final state of a quantum system given an initial state. The method can serve as a starting point for additional refinements that lead to new pulses with improved properties. Among others, we propose an algorithm to design pulses that transfer population in a reversible manner between given initial and final states of coupled fixed-frequency superconducting qubits.

DOI: 10.1103/PhysRevA.99.052316

I. INTRODUCTION

Methods to shape pulses [1] that control quantum processes have allowed important advances in different domains, ranging from the steering of photochemical processes [2–4] to the optimization of gate operations in quantum computing [5,6].

In quantum information, optimal control theory (OCT) is typically used to generate target unitary operators [5,7–10]. Within the field of superconducting qubits [11] OCT has been successfully applied to design various qubit gates in different hardware implementations [6,12–15] as well as to identify optimal operating conditions, such as the quasidispersive regime [16].

In parallel to OCT, local control theory (LCT) has also emerged as a valuable approach to control the dynamics of quantum systems by shaping external fields. In particular, LCT has already been successfully applied to steer photochemical reactions in molecular systems [17–19]. In LCT, an external field is designed on-the-fly under the constraint that it monotonically increases the quantum population of a selected target state when starting from a given initial state [20,21]. While OCT is based on a computationally intensive variational approach, which requires computing the full time evolution of the system at each optimization step, LCT can generate pulses that produce the desired population transfer by computing the evolution of the system only once. Although LCT does not necessarily provide a time-optimal pulse, thanks to its remarkable computational efficiency and conceptual simplicity, it can nonetheless become the method of choice for the design of state-preparation pulses.

In this paper, we focus on the application of LCT to generate state-preparation pulses for fixed-frequency superconducting qubits coupled via tunable couplers. In Sec. II we introduce LCT and show how to apply it to a setup made up of fixed-frequency transmon qubits coupled by a tunable coupler [22,23]. Section III A presents and discusses the pulses generated by the LCT algorithm. Sections III B–III D report on a procedure aimed at further optimizing their properties such as bandwidth, pulse length, and reversibility.

II. METHODS

A. Theoretical background

We consider n fixed-frequency qubits all mutually interacting through a single flux-tunable qubit, called a tunable coupler (TC) [22]. Such systems combine the long coherence time of fixed-frequency transmon qubits with the high controllability of flux-tunable coupling elements. The system is described by the Hamiltonian [23]

$$\begin{aligned}\hat{H}(t) = &\sum_{i=1}^{n} \omega_i \hat{a}_i^\dagger \hat{a}_i - \alpha_i (1 - \hat{a}_i^\dagger \hat{a}_i)\hat{a}_i^\dagger \hat{a}_i \\ &+ \omega_{\mathrm{TC}}(t)\hat{a}_{\mathrm{TC}}^\dagger \hat{a}_{\mathrm{TC}} - \alpha_{\mathrm{TC}}(1 - \hat{a}_{\mathrm{TC}}^\dagger \hat{a}_{\mathrm{TC}})\hat{a}_{\mathrm{TC}}^\dagger \hat{a}_{\mathrm{TC}} \\ &+ \sum_{i=1}^{n} g_i (\hat{a}_i^\dagger + \hat{a}_i)(\hat{a}_{\mathrm{TC}}^\dagger + \hat{a}_{\mathrm{TC}}), \end{aligned} \tag{1}$$

in units of $\hbar = 1$. The qubit i and TC creation and annihilation operators are $\hat{a}_i^\dagger$, $\hat{a}_i$, $\hat{a}_{\mathrm{TC}}^\dagger$, and $\hat{a}_{\mathrm{TC}}$, respectively. Qubit i has frequency ω_i, anharmonicity α_i, and couples with strength g_i to the TC. The frequency of the TC, $\omega_{\mathrm{TC}}(t)$, is controlled by a current $I(t)$ brought close to the TC by a high-speed flux-bias line; see Fig. 1(a). The resulting flux $\Phi(t)$ threading through the TC SQUID loop changes the frequency of the TC according to

$$\omega_{\mathrm{TC}}(t) = \omega_{\mathrm{TC}}^0 \sqrt{|\cos(\pi \Phi(t)/\Phi_0)|}, \tag{2}$$

*ita@zurich.ibm.com

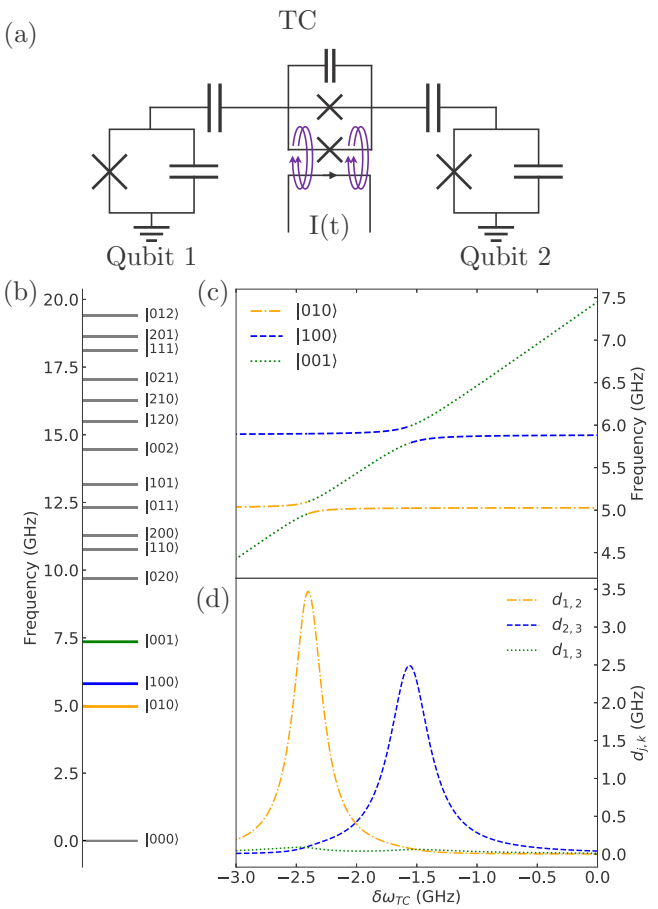

FIG. 1. (a) Sketch of two fixed-frequency transmon qubits coupled by using a tunable coupler. (b) Energy levels of the undriven system for states up to 20 GHz above the ground state. (c) Evolution of the eigenstates of the full Hamiltonian in Eq. (1) as a function of $\delta\omega_{\rm TC}$. The labels $|010\rangle$ (orange), $|100\rangle$ (blue), and $|001\rangle$ (green) refer to the eigenstates of the Hamiltonian when the coupling is set to zero. (d) The nonadiabatic couplings $d_{1,2}$ (orange dash-dotted line), $d_{2,3}$ (blue dashed line), and $d_{1,3}$ (green dotted line), as functions of $\delta\omega_{\rm TC}$.

where Φ_0 is the magnetic flux quantum [24]. The full system wave function $|\Psi(t)\rangle$ then evolves according to the time-dependent Schrödinger equation

$$i\partial_t\,|\Psi(t)\rangle = \hat{H}(t)\,|\Psi(t)\rangle\,. \tag{3}$$

The population $\langle\hat{P}_\phi\rangle$ of any n-qubit target state $|\phi\rangle$ is governed by

$$\partial_t\langle\hat{P}_\phi\rangle = i\langle[\hat{H}(t),\hat{P}_\phi]\rangle, \tag{4}$$

where $\hat{P}_\phi = |\phi\rangle\langle\phi|$ is the corresponding projector operator and $\langle\dots\rangle$ denotes the expectation value with respect to $|\Psi(t)\rangle$. In our model, the only free, tunable parameter is the frequency of the tunable coupler $\omega_{\rm TC}(t)$. We will, thus, employ LCT to increase the population in $|\phi\rangle$ by shaping $\omega_{\rm TC}(t)$ on the fly. The TC frequency can be decomposed into a time-independent and a time-dependent part $\omega_{\rm TC}(t) = \omega_{\rm TC} + \delta\omega_{\rm TC}(t)$ [19,21]. This splits the Hamiltonian $\hat{H}(t)$ into a time-dependent term $\hat{H}'(t) = \delta\omega_{\rm TC}(t)\hat{a}^\dagger_{\rm TC}\hat{a}_{\rm TC}$ and a drift term

$$\begin{aligned}\hat{H}_{\rm d} = &\sum_{i=1}^{n}\omega_i\hat{a}_i^\dagger\hat{a}_i - \alpha_i(1-\hat{a}_i^\dagger\hat{a}_i)\hat{a}_i^\dagger\hat{a}_i\\ &+\omega_{\rm TC}\hat{a}^\dagger_{\rm TC}\hat{a}_{\rm TC} - \alpha_{\rm TC}(1-\hat{a}^\dagger_{\rm TC}\hat{a}_{\rm TC})\hat{a}^\dagger_{\rm TC}\hat{a}_{\rm TC}\\ &+\sum_{i=1}^{n} g_i(\hat{a}_i^\dagger+\hat{a}_i)(\hat{a}^\dagger_{\rm TC}+\hat{a}_{\rm TC}).\end{aligned} \tag{5}$$

The drift $\omega_{\rm TC}$ term depends on the constant dc flux bias applied to the TC [22]. When the target state $|\phi\rangle$ is an eigenvector $|\psi_j\rangle$ of the drift Hamiltonian $\hat{H}_{\rm d}$ the projector operator $\hat{P}_\phi$ commutes with $\hat{H}_{\rm d}$ and Eq. (4) simplifies to

$$\partial_t\langle\hat{P}_j\rangle = i\delta\omega_{\rm TC}(t)\langle[\hat{a}^\dagger_{\rm TC}\hat{a}_{\rm TC},\hat{P}_j]\rangle. \tag{6}$$

LCT induces a monotonic increase of the target-state population by generating a $\delta\omega_{\rm TC}(t)$ pulse that guarantees the positivity of the right-hand side of Eq. (6). For our setup this condition is achieved by changing the frequency of the TC according to

$$\delta\omega_{\rm TC}(t) = -i\lambda\langle[\hat{a}^\dagger_{\rm TC}\hat{a}_{\rm TC},\hat{P}_j]\rangle^*. \tag{7}$$

The coupling parameter λ controls the magnitude by which the control field $\delta\omega_{\rm TC}(t)$ is changed. Its value can be tuned as long as the resulting pulse $\delta\omega_{\rm TC}(t)$ can be implemented in realistic experimental setups.

A projector made of an arbitrary linear combination of drift-Hamiltonian eigenstates does not, in general, commute with the drift Hamiltonian. Therefore, such a linear combination of eigenstates cannot be used as a target state in our formulation of LCT since an equivalent to Eq. (7) cannot be obtained. Thus the current formulation of the LCT algorithm can only generate pulses for population transfer between pure drift Hamiltonian eigenstates.

When some of the (high energy) states do not contribute to the dynamics, we can simplify the simulation by restricting the action of the LCT algorithm to a subspace of the full Hilbert space by using the projector operator $\hat{P}_{n'} = \sum_{k=1}^{n'}|\psi_k\rangle\langle\psi_k|$ over the first n' eigenvectors (assumed to be ordered according to their corresponding eigenvalues). Equation (7) then simplifies to

$$\delta\omega_{\rm TC}(t) \simeq 2\lambda\,{\rm Im}\left(\sum_k^{n'}\langle\psi_j|\hat{a}^\dagger_{\rm TC}\hat{a}_{\rm TC}|\psi_k\rangle\langle\psi_k|\Psi(t)\rangle\langle\psi_j|\Psi(t)\rangle^*\right). \tag{8}$$

Since the TC frequency cannot exceed $\omega^0_{\rm TC}$, see Eq. (2), $\delta\omega_{\rm TC}(t)$ is confined to the interval $[-\omega^0_{\rm TC}, 0]$. Thus, it is necessary to impose a restriction on the λ factor to avoid reaching the upper bound of $\delta\omega_{\rm TC}(t)$. This is accomplished by capping the value of $\delta\omega_{\rm TC}(t)$ to zero (i.e., taking $\min[\delta\omega_{\rm TC}(t), 0]$) and by constraining the magnitude of λ such as $\delta\omega_{\rm TC}(t) > -\omega^0_{\rm TC}$.

The LCT algorithm can be summarized in two steps: First, the instantaneous state is propagated for a short time interval $[t, t+\delta t]$ under $\hat{H}(t)$. Second, the resulting wave function $|\Psi(t+\delta t)\rangle$ is used to update the external field following Eq. (8). These two steps are repeated using the updated control field until the desired population transfer is achieved.

A smooth external driving pulse is obtained when δt is made sufficiently small. For practical purposes, when the target state $|\phi\rangle$ does not overlap with the initial system wave function $|\Psi(0)\rangle$, a small fraction η of the target state is added into the initial wave function,

$$|\Psi'(0)\rangle = \sqrt{\eta}\,|\psi_j\rangle + \sqrt{1-\eta}\,|\Psi(0)\rangle\,, \tag{9}$$

to ensure that the LCT algorithm converges. Since LCT pulses are directly constructed from an evolving wave function, they are very sensitive to perturbations of the system parameters and have to be designed for each system individually.

B. System

We apply LCT to systems composed of $n = 2$, 3, and 4 qubits; see Eq. (1) and Fig. 1(a). In the two-qubit system [22], the qubits, labeled Q1 and Q2, have frequencies $\omega_1/(2\pi) = 5.890$ GHz and $\omega_2/(2\pi) = 5.031$ GHz, respectively, and anharmonicities $\alpha_1/(2\pi) = -324$ MHz and $\alpha_2/(2\pi) = -235$ MHz, respectively. They are coupled with strengths $g_1/(2\pi) = 100$ MHz and $g_2/(2\pi) = 71$ MHz, respectively, to a TC with a maximum frequency $\omega_{\rm TC}^0/(2\pi) = 7.445$ GHz. We chose the value of the TC anharmonicity to be $\alpha_{\rm TC}/(2\pi) = -280$ MHz, consistent with the value reported in Ref. [23]. The control pulses are designed so that $\delta\omega_{\rm TC}$ is zero at the beginning and end of the simulation. We found that the system can be accurately described by using only the first three states of the qubits and of the TC since the higher-energy states do not affect the population transfer between the states $|0\rangle$ and $|1\rangle$ of Q1 and Q2. The eigenvectors of the drift Hamiltonian in Eq. (5), labeled $|q_1q_2q_{\rm TC}\rangle$, are used to identify the 27 system states; see Fig. 1(b). Due to the modest size of the problem, we do not need to introduce projectors as described in Eq. (8). When $\delta\omega_{\rm TC}$ is swept from 0 to -3 GHz, we observe two avoided-level crossings between the TC state and the qubit states; see Fig. 1(c). The associated nonadiabatic coupling terms, obtained with the Hellmann–Feynman expression[1] are shown in Fig. 1(d). The LCT algorithm makes use of these avoided-level crossings to transfer population between the two qubits.

In systems composed of $n = 3$ and $n = 4$ qubits, the frequencies of qubits Q3 and Q4 were equidistantly interpolated between the Q1 and Q2 frequencies, giving $\omega_3/(2\pi) = 5.461$ GHz in the three-qubit system, and $\omega_3/(2\pi) = 5.317$ GHz and $\omega_4/(2\pi) = 5.604$ GHz in the four-qubit system. This ensures that the energies of the single-excited states of the third and fourth qubits are equidistantly located between the first energy levels of Q1 and Q2. All corresponding coupling and anharmonicity values for the third and fourth qubit are set to the values of g_1 and α_1. Again, only the first three lowest states for each qubit and TC prove sufficient to accurately model the population transfer between pure single excited qubit states in $n = 3$ and $n = 4$ qubits systems.

[1]The nonadiabatic coupling terms d_{jk} between pairs of the full system eigenstates $|\psi_j\rangle$ and $|\psi_k\rangle$ [see Eq. (1)] with the corresponding eigenenergies $\varepsilon_j(\delta\omega_{\rm TC})$ and $\varepsilon_k(\delta\omega_{\rm TC})$ are determined with the Hellmann–Feynman expression [25]

$$d_{jk}(\delta\omega_{\rm TC}) = \frac{\langle\psi_j(\delta\omega_{\rm TC})|\frac{\partial\hat{H}(\delta\omega_{\rm TC})}{\partial\delta\omega_{\rm TC}}|\psi_k(\delta\omega_{\rm TC})\rangle}{\varepsilon_j(\delta\omega_{\rm TC}) - \varepsilon_k(\delta\omega_{\rm TC})}.$$

III. RESULTS AND DISCUSSION

A. Local control theory pulse

In this section, we design a LCT pulse that transfers population from the state $|100\rangle$ to the state $|010\rangle$, i.e., that brings the excitation from Q1 to Q2 in a $n = 2$ qubits system. We assume that the TC is biased at the flux sweet spot $\Phi(t = 0) = 0$. Since the initial and final states are orthonormal, we use the state preparation in Eq. (9) with $\eta = 10^{-6}$ to initialize the LCT algorithm.

Figure 2(a) shows a 150-ns-long LCT pulse obtained for $\lambda = 12\,500$. This pulse makes the tunable coupler energy level oscillate between the two avoided level-crossings depicted in Fig. 1(c). As the TC $|001\rangle$ state passes through the first avoided crossing at -1.56 GHz a fraction of the qubit population in $|100\rangle$ is transferred to the TC. Part of this population is then transferred to the second qubit (state $|010\rangle$) once the second avoided crossing at -2.40 GHz is reached. The TC oscillates with a complicated frequency pattern dominated by the harmonics of the transition between the two qubits, $(\omega_1 - \omega_2)/(2\pi) = 859$ MHz and by other components below 1 GHz as shown by the power spectrum of the pulse in Fig. 2(c). These frequencies populate several higher-energy states, most notably states $|201\rangle$, $|021\rangle$, $|210\rangle$, and $|111\rangle$. However, none of these states reach a population grater than 10^{-5} and all rapidly depopulate below 10^{-7} by the time the pulse ends. Only about 2×10^{-6} population remains in the $|102\rangle$ excited state at the end of the pulse. As expected from Eqs. (6) and (7), after an initial delay $t_{\rm on}$ of 160 ns, the population of the target state $|010\rangle$ increases monotonically with time while the populations of the other states rapidly oscillate. After $\sim$300 ns the initial population has been almost entirely transferred to the target state. Only a population of 2×10^{-6} is left in the initial state, which, together with the remaining population in the $|102\rangle$ state, gives a mismatch $1 - \langle P_{|010\rangle}\rangle$ of $\sim 4 \times 10^{-6}$, where $\langle P_{|010\rangle}\rangle$ is the population of the target state. Increasing the value of the λ parameter increases the fidelity (see Appendix A). While very promising, this first "high fidelity" LCT pulse has a complex spectrum and would require instruments with a large bandwidth.

B. Optimization of local control theory pulses

Limits set by the control instruments make large-bandwidth pulses impractical. We therefore need a procedure to refine the LCT pulse, which confines the bandwidth to a reasonable range. To this end, we apply a high-frequency filter to the LCT pulse obtained in the previous section and use it as a "reference" to generate an improved pulse using the LCT algorithm. This new reference corresponds to the term $\delta\omega_{\rm TC}^{\rm filt}(t)$ in Eq. (10). In practice, we decompose the new LCT pulse into three different components

$$\omega_{\rm TC}(t) = \omega_{\rm TC}^0 + \delta\omega_{\rm TC}^{\rm filt}(t) + \delta\omega_{\rm TC}^{\rm lct,2}(t). \tag{10}$$

Only the component $\delta\omega_{\rm TC}^{\rm lct,2}(t)$, initially set to zero, will be generated on the fly by using the LCT algorithm, while the first two terms are kept fixed. As in the previous section,

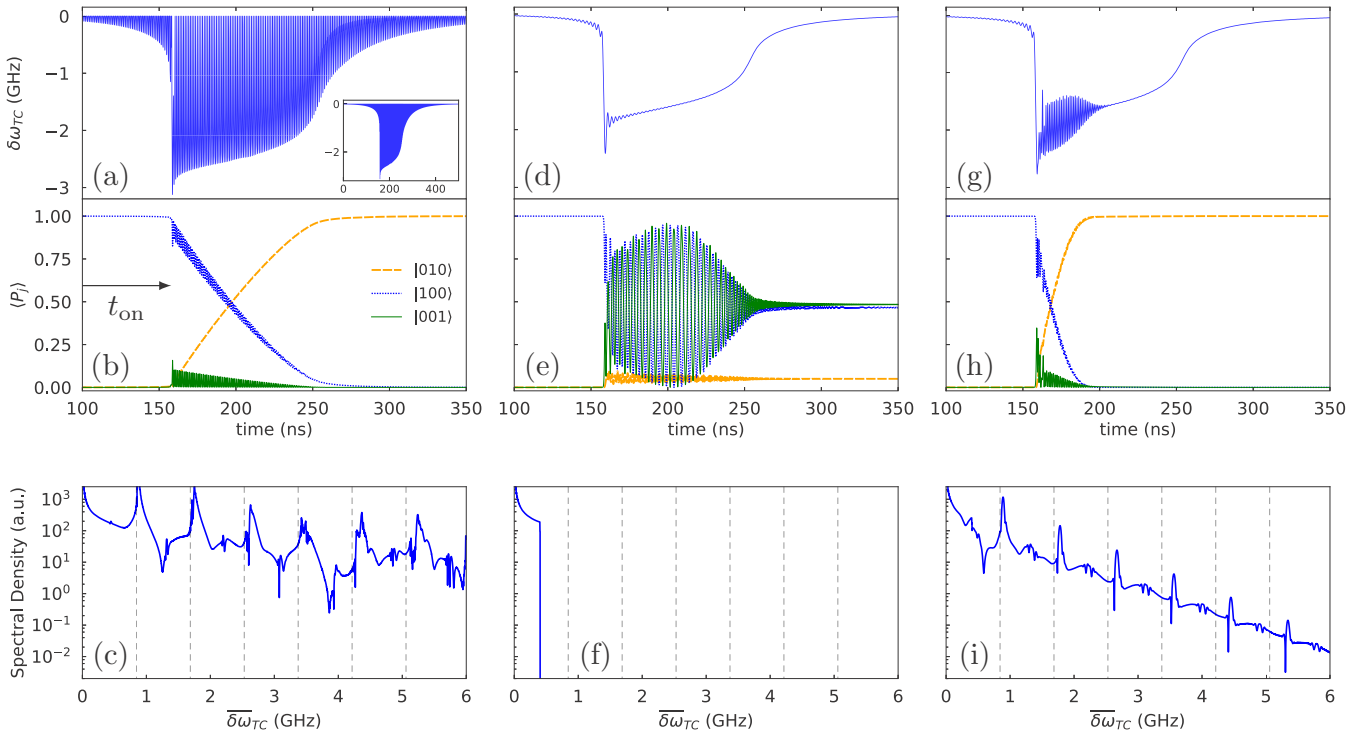

FIG. 2. (a) LCT pulse designed to transfer population from state $|100\rangle$ to state $|010\rangle$ (inset shows the full 450 ns pulse). The parameter λ was set to 12 500. (d) Frequency-filtered pulse $\delta\omega_{\rm TC}^{\rm filt}(t)$ used as an initial condition to design the second local control pulse. (g) LCT pulse designed to transfer population from state $|100\rangle$ to state $|010\rangle$ when using the pulse in panel (d) as an initial condition. (b), (e), (h) Population transfer resulting from the pulses in panels (a), (d), and (g), respectively. (c), (f), (i) Fourier transforms of the pulses in panels (a), (d), and (g), respectively. The dashed lines indicate the harmonics corresponding to frequency differences between the qubits.

the pulse $\delta\omega_{\rm TC}^{\rm lct,2}$ is shaped by using the requirement that the right-hand side of Eq. (6), $\partial_t \langle \hat{P}_j \rangle$, remains positive.

The filtered pulse $\delta\omega_{\rm TC}^{\rm filt}(t)$ in Fig. 2(d) is obtained by applying a high-frequency cutoff at 0.4 GHz to the pulse in Fig. 2(a). The corresponding spectra before and after the application of the filter are shown in Figs. 2(c) and 2(f), respectively. This operation removes much of the complex structure of the pulse while preserving its overall shape [Fig. 2(d)]. As expected, the pulse made up of the first two components in Eq. (10) fails to transfer the population to the target qubit [Fig. 2(e)]. However, using LCT we generate a new time-dependent field, i.e., $\delta\omega_{\rm TC}^{\rm lct,2}(t)$ in Eq. (10), with a coupling parameter λ_2 to restore the population transfer. In particular, we are able to design new LCT pulses with a narrow bandwidth and an error $1 - \langle P_{|010\rangle} \rangle < 10^{-6}$ using λ_2 values in the interval [100, 1000]; see Figs. 2(g)–2(i). In addition, the population transfer is now completed in only ∼30 ns [see Fig. 2(h)] compared with the initial 120 ns obtained with the first LCT run described in Sec. III A [Fig. 2(b)]. Although some higher-energy states are excited at the pulse onset, their population never exceeds 10^{-5} and returns to values below 10^{-7} before the end of the pulse. This improvement is due to the reference pulse, i.e., the sum $\omega_{\rm TC}^0 + \delta\omega_{\rm TC}^{\rm filt}(t)$, forcing the TC frequency in the energy range that matches the separation between the two avoided-level crossings shown in Fig. 1(c). Note that truncating the power spectrum in Fig. 2(i) above 1 or 1.5 GHz without further optimization will reduce the fidelity to 10^{-4} and 10^{-5}, respectively.

C. Reverse processes

So far, our LCT pulses accomplish a well-defined population transfer from a given initial state to a final state. Therefore, we do not expect that applying the same pulse to the final state reverses the process and transfers the population back to the initial state. For instance, applying the pulse in Fig. 2(a) (generated to transfer population from $|100\rangle$ to $|010\rangle$) to the reverse process (from $|010\rangle$ back to $|100\rangle$) only achieves an imperfect transfer that leaves 3% of the population in the TC. Interestingly, we found that the amount of population trapped in the TC is particularly sensitive to the value of λ_2. Therefore, the LCT pulse can be further optimized to increase the efficiency of the reverse transfer by tuning λ_2. Changes to λ_2 do not affect the success of the population transfer from $|100\rangle$ to $|010\rangle$, since the initial and final states and the reference pulse $\delta\omega_{\rm TC}(t)$ are unchanged. They also do not affect the population of the high-energy states. We exploit these facts in an iterative procedure we developed that optimizes both the direct and reverse population transfers between the states $|100\rangle$ and $|010\rangle$. The initial pulse is the bandwidth-optimized pulse derived in Sec. III B. For an initial choice of λ_2, we derive a first LCT pulse for the direct process ($|100\rangle$ to $|010\rangle$) and then test it for the reverse transfer ($|010\rangle$ to $|100\rangle$). If this fails to transfer the population back to the initial state $|100\rangle$ with an error $1 - \langle P_{|100\rangle} \rangle$ less than 10^{-6} we update the parameter λ_2 and recompute the pulse by using the LCT algorithm. This procedure is repeated until the reverse population transfer fidelity reaches a maximum. The

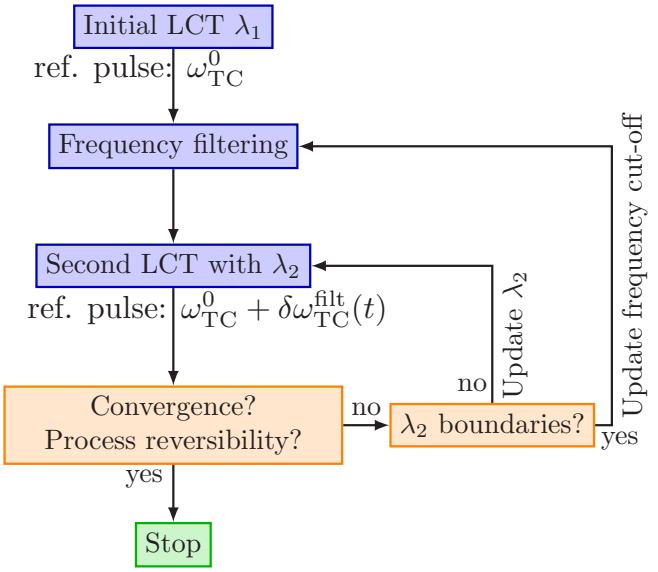

FIG. 3. Flow chart showing the iterative procedure used to obtain pulses with a smaller bandwidth and capable of transferring population when the initial and target states are exchanged. A new LCT calculation is performed each time the parameter λ_2 is updated or when a new frequency cutoff is applied.

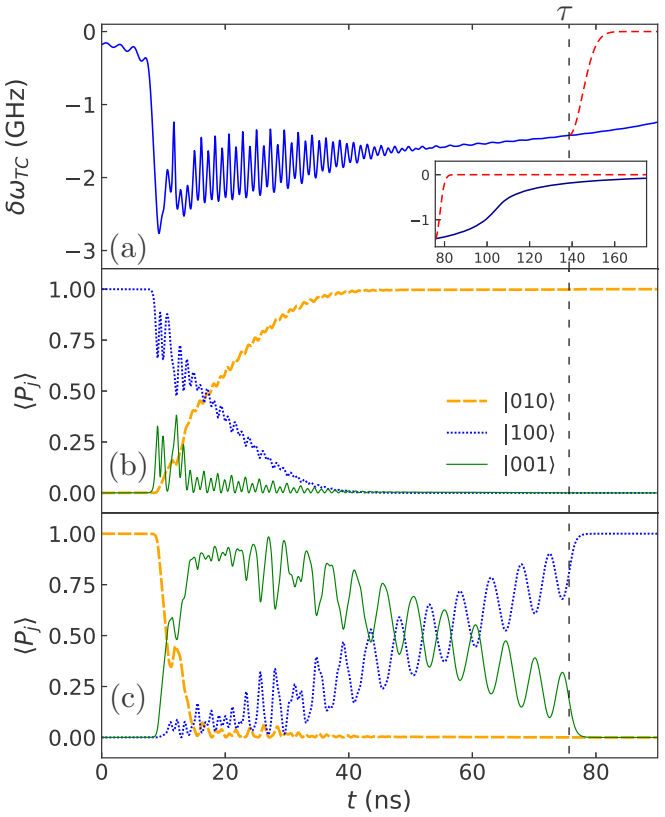

FIG. 4. (a) Final pulse generated by the algorithm depicted in Fig. 3 (final frequency cut-off at 0.45 GHz, $\lambda_2 = 437.4$). The inset shows the tail of the pulse (after the time τ), which can be substituted with the half-Gaussian function (dashed red line). (b) Evolution of the system when all the population is initially in Q1. (c) Evolution of the system when all the population is initially in Q2. The populations shown in panels (b) and (c) are calculated by using the pulse with the shortened tail.

Nelder–Mead algorithm [26] is used to optimize λ_2. In some cases, we noticed that maximizing the population transferred during the reverse process required changing the frequency cutoff for $\delta\omega_{\rm TC}^{\rm filt}(t)$. A flow chart of the algorithm used to obtain a narrow-bandwidth pulse able to transfer the qubit population in both directions is shown in Fig. 3. For the setup in Fig. 1 and the parameter discussed in Sec. II B, the produced LCT pulse is given in Fig. 4(a) together with the population dynamics for the direct and reverse processes respectively shown in Figs. 4(b) and 4(c). The final LCT pulse in Fig. 4(a) can further be used to inspire a new class of fully analytical and ultrashort pulses that can be used for state preparation (see Appendix C).

D. Pulse truncation

The pulses obtained by using the algorithm shown in Fig. 3 still have a long tail in the time domain that is inherited from the original, fixed λ, LCT calculation (Sec. III A). Since the tail does not contribute to the population transfer, see e.g., Fig. 2(h), the pulses can be shortened by imposing a Gaussian decay after a critical time τ using the half-Gaussian function $\alpha \exp\{-(t-\tau)^2/(2\sigma^2)\}$ for $t \geqslant \tau$ shown in Fig. 4(a). The optimal value of τ is obtained by including it in the optimization process shown in Fig. 3, while its initial value is selected as the time required by the original pulse in Fig. 4(a) to reach 99% of population transfer for the reverse process in Fig. 4(c). For a chosen σ value, this leads to an optimized pulse capable of transferring population in both directions with both fidelities less than 10^{-6}. The α parameter is always chosen to guarantee continuity at the transition point.

E. Local control theory in three- and four-qubit systems

We applied LCT to systems with three and four qubits coupled to the TC. LCT pulses were constructed for direct population transfers between neighboring and non-neighboring states with one excitation. The envelope of all the obtained pulses are similar to the envelope of the LCT pulse designed for the two-qubit system. However, the spectrum of the pulses is different and is dominated by the energy difference between the initial and final states. Because the third and fourth qubit frequencies were positioned between the frequencies of Q1 and Q2, the energy separation between all the single-excited states is reduced. Consequentially, the nonadiabatic coupling terms are increased, especially between non-neighboring states (see an example of a fixed-frequency four-qubit system in Appendix B). As the TC frequency oscillates between the energy of Q1 and Q2, larger population deposits are made into the states neighboring the target state. This reduces the fidelity of the pulse. In the three-qubit system, where the single-excited states are mutually separated by ∼0.43 GHz, fidelities of the order 10^{-5}, expressed as $1 - \langle P_j \rangle$ where $\langle P_j \rangle$ is the final population of the target eigenstate, are achieved. In the four-qubit system, population transfers

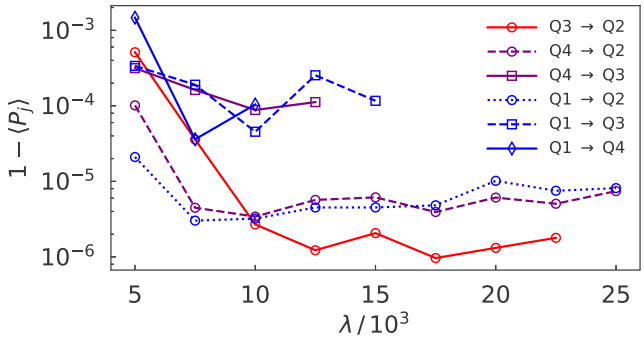

FIG. 5. Fidelities (expressed as $1-\langle P_j\rangle$ where j is the target state) of LCT pulses for population transfers between single-excited states in a four-qubit system (see definition of states in Appendix B) generated for a variety of λ parameters. The frequencies of the qubits are 5.890, 5.031, 5.317, and 5.604 GHz for qubits Q1–Q4, respectively. Only points corresponding to λ parameters that gave acceptable LCT pulses are shown.

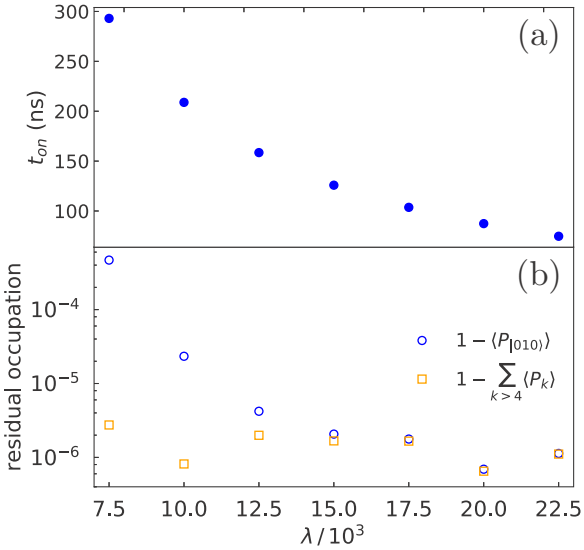

FIG. 6. (a) Dependency of the LCT pulse-onset time on the λ parameter in the two-qubit system. (b) LCT pulse fidelity $1-\langle P_{|010\rangle}\rangle$ (blue hollow circles) as function of the λ parameter. The total occupation of all the states above $|001\rangle$ (see Fig. 1) is shown by hollow orange squares.

between single-excited states with higher frequencies achieve fidelities between 10^{-3} and 10^{-4}, while population transfers between single-excited states with lower frequencies achieve fidelities between 10^{-5} and 10^{-6} (see Fig. 5). The observed trend shows how the increased nonadiabatic couplings caused by frequency crowding affect the pulses generated using LCT. During our research, we observed that using the optimization procedure shown in Fig. 3 does not improve the fidelities in either the three- or four-qubit systems. Running the LCT algorithm more than once does not materially improve the pulse fidelity.

IV. CONCLUSION

In this work we use LCT to manipulate qubit populations in an architecture where fixed-frequency superconducting qubits are coupled by using tunable couplers. Given an initial state and a target state, LCT constructs a pulse on the fly by computing the time evolution once. The only tunable parameter is the intensity of the applied pulse. λ influences the shape and length of the resulting LCT pulse, giving the possibility to shorten the transfer time below 50 ns while keeping fidelity above 0.9999.

The LCT algorithm was extended to design pulses that can achieve a complete population transfer in both directions between the initial and target states. This extension of the LCT algorithm comprises an additional optimization step over the parameter λ. LCT can also serve as a starting point for a deterministic procedure to further reduce the complexity of the pulse; see Appendix C. This may open a new avenue of research to design efficient gates for different applications of quantum computing [27–29].

LCT experiences difficulties with certain transitions in frequency-crowded systems, e.g., three- and four-qubits coupled to one TC, due to population leakage into neighboring states around the initial and target states. Further work will investigate ways to mitigate these issues.

ACKNOWLEDGMENTS

The authors acknowledge stimulating discussions with Marco Roth and Nikolaj Moll. We also acknowledge generous computational time from the Croatian National Grid Infrastructure (CRO-NGI) and the Irish Centre for High–End Computing (ICHEC). This work received funding from the European Union's Horizon 2020 research and innovation program under the Grant Agreement No. 676531 (Project E-CAM).

APPENDIX A: DEPENDENCY OF LOCAL CONTROL THEORY PULSE-ONSET TIME AND FIDELITY ON THE λ PARAMETER

The two-qubit system evolution was propagated up to 500 ns after which the pulse fidelity was calculated as $1-\langle P_{|010\rangle}\rangle$, where $\langle P_{|010\rangle}\rangle$ is the final population in the target state. The pulse-onset time t_{on} is defined as the time at which LCT creates a sudden increase in the pulse amplitude and the rate at which population is transferred to the target state. Larger λ-parameter values give proportionally larger transfer rates and decrease t_{on} [see Fig. 6(a)]. Shorter t_{on} times result in shorter pulses with less population remaining in the TC ($|001\rangle$ state), therefore giving better population transfer fidelities [see Fig. 6(b)]. However, the pulse fidelity also depends on the total population remaining in the states above $|001\rangle$. This population does not depend on the λ parameter. For λ parameters greater than 25 000, LCT produces pulses with a sudden rise in amplitude that approaches or exceeds the $-\omega_{\mathrm{TC}}^0$ value. Such unphysical pulses were discarded. Similar effects are observed in the three- and four-qubit systems.

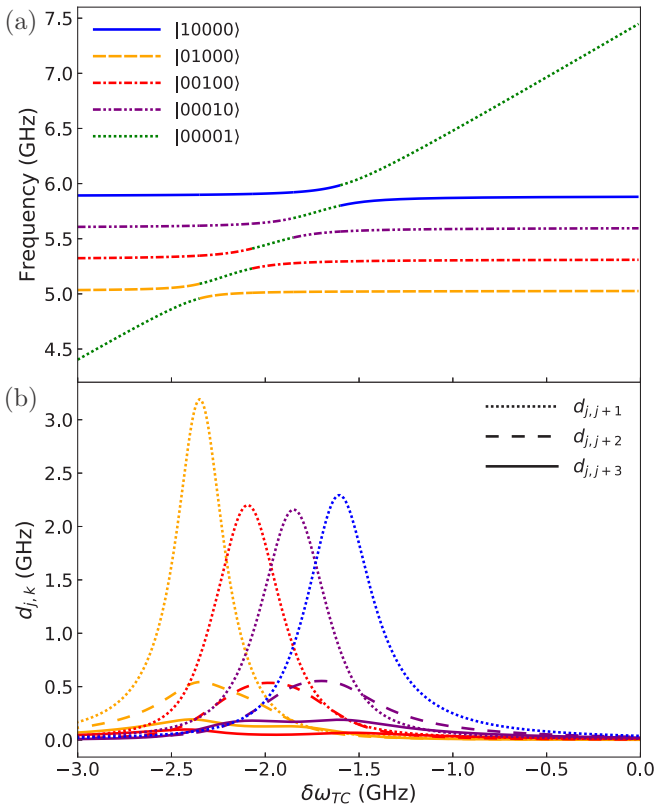

FIG. 7. (a) Frequency of the single-excited eigenstates of the fixed-frequency four-qubit Hamiltonian, see Eq. (1), as a function of $\delta\omega_{\mathrm{TC}}$. Within the $|q_1q_2q_3q_4q_{\mathrm{TC}}\rangle$ state nomenclature, colors and line styles (see legend) indicate states with characters $|10000\rangle$ (blue), $|01000\rangle$ (orange), $|00100\rangle$ (red), $|00010\rangle$ (violet), and $|00001\rangle$ (green). Note the change of state characters at the avoided crossings. (b) The nonadiabatic couplings between all pairs of states depicted in panel (a). Dotted lines indicate nonadiabatic couplings between neighboring pairs of states $(j, j+1)$, while dashed and full lines do the same between $j, j+2$ and $j, j+3$ pairs of states, respectively.

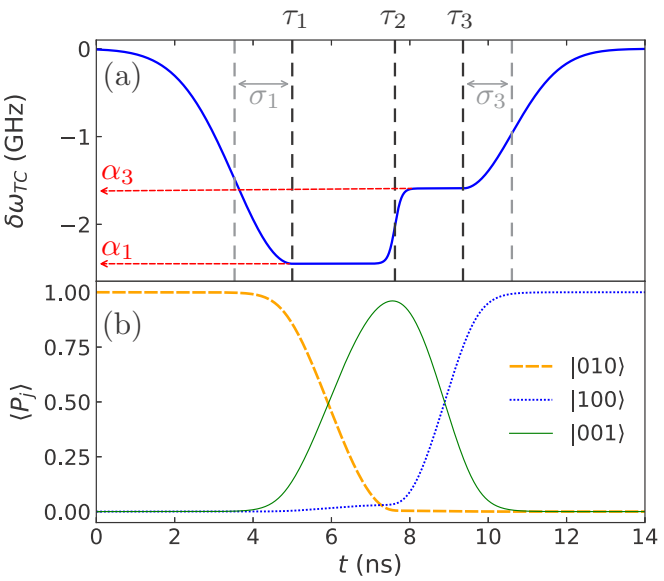

FIG. 8. (a) Time-optimal pulse shape obtained from Eq. (C1) accomplishing the $|010\rangle \rightarrow |100\rangle$ transfer by using the TC $|001\rangle$. The optimal parameter values are $\alpha_1 = -2.449$ GHz, $\alpha_3 = -1.590$ GHz, $\tau_1 = 5.0$ ns, $\tau_2 = 7.62$ ns, $\tau_3 = 9.36$ ns, $\sigma_1 = 1.47$ ns, $\sigma_2 = 0.17$ ns, $\sigma_3 = 1.25$ ns. (b) Evolution of the populations during the pulse shown in panel (a).

APPENDIX B: STATE ENERGIES AND NONADIABATIC COUPLINGS OF A FIXED-FREQUENCY FOUR-QUBIT SYSTEM

Adding Q3 and Q4 to the two-qubit system does not significantly perturb the single-excited states of Q1 and Q2 [compare Fig. 7(a) with Fig. 1(c)]. However, the nonadiabatic coupling terms between non-neighboring states ($j, j+2$ and $j, j+3$) significantly increase [compare Fig. 7(b) with Fig. 1(d)], resulting in population leakage during the LCT pulses to states in the vicinity of the initial and target states.

APPENDIX C: ANALYTIC STATE-PREPARATION PULSE

Larger nonadiabatic coupling terms enable a faster population transfer. We exploit this to construct a shorter analytic pulse for the two-qubit system. This pulse drives the TC into regions where the nonadiabatic coupling is large. Inspired by the numerical pulse shown in Fig. 4(a), we construct a new pulse

$$\delta\omega_{\mathrm{TC}}(t) = \begin{cases} \alpha_1 \exp\left[-\frac{1}{2}\left(\frac{t-\tau_1}{\sigma_1}\right)^2\right], & t < \tau_1 \\ \frac{1}{2}(\alpha_3 + \alpha_1) & \\ +\frac{1}{2}(\alpha_3 - \alpha_1)\tanh\left(\frac{t-\tau_2}{\sigma_2}\right), & \tau_1 \leqslant t \leqslant \tau_3 \\ \alpha_3 \exp\left[-\frac{1}{2}\left(\frac{t-\tau_3}{\sigma_3}\right)^2\right], & t > \tau_3 \end{cases} \quad \text{(C1)}$$

that reduces the duration of the state preparation. Here α_i are the amplitudes and σ_1 and σ_3 are the decay times of two half-Gaussian pulse envelopes connected by a switching function with a slope controlled by σ_2; see Fig. 8(a). The values of these parameters were obtained by using an optimization-with-bounds procedure from the sequential least square programming algorithm [30], which enforces a complete population transfer from $|010\rangle$ to $|100\rangle$. For the initial conditions, the values of α_1 and α_3 were set equal to the energies of the second and first avoided crossings, respectively, while $\tau_2 - \tau_1$ and $\tau_3 - \tau_1$ were set to the times needed by a LCT designed pulse to transfer the population from $|010\rangle \rightarrow |001\rangle$ [see Fig. 4(c)] and $|100\rangle \rightarrow |010\rangle$ [see Fig. 4(b)], respectively. In our simulations, τ_1, chosen arbitrarily, was set to 5 ns. Initial σ_i parameters were set close to zero and relaxed during a second optimization step once the α and τ values were fully determined. This yields a smooth pulse, shown in Fig. 8(b), which sequentially transfers the population from Q2 to TC and finally to Q1 with a total fidelity $1 - \langle P_{|100\rangle}\rangle < 10^{-6}$. The reverse population transfer (from Q1 to Q2 via the TC) is achieved by inverting the pulse in the time domain. This pulse is similar to the case where frequency-tunable elements are

used to shuttle population to and from different elements in a larger quantum system [31]. Interestingly, the final pulse duration is short (∼14 ns) compared with the coherence times in state-of-the-art experiments.

[1] S. J. Glaser, U. Boscain, T. Calarco, C. P. Koch, W. Köckenberger, R. Kosloff, I. Kuprov, B. Luy, S. Schirmer, T. Schulte-Herbrüggen, D. Sugny, and F. K. Wilhelm, Eur. Phys. J. D **69**, 279 (2015).

[2] M. Shapiro and P. Brumer, *Principles of the Quantum Control of Molecular Processes* (Wiley-Interscience, New York, 2003).

[3] G. G. Balint-Kurti, S. Zou, and A. Brown, Optimal control theory for manipulating molecular processes, in *Advances in Chemical Physics* (John Wiley & Sons, Inc., Hoboken, NJ, 2008), Vol. 138, pp. 43–94.

[4] I. R. Sola, B. Y. Chang, S. A. Malinovskaya, and V. S. Malinovsky, Adv. At., Mol., Opt. Phys. **67**, 151 (2018).

[5] N. Khaneja, T. Reiss, C. Kehlet, T. Schulte-Herbrüggen, and S. J. Glaser, J. Magn. Reson. **172**, 296 (2005).

[6] F. Motzoi, J. M. Gambetta, P. Rebentrost, and F. K. Wilhelm, Phys. Rev. Lett. **103**, 110501 (2009).

[7] T. Caneva, T. Calarco, and S. Montangero, Phys. Rev. A **84**, 022326 (2011).

[8] J. Kelly, R. Barends, B. Campbell, Y. Chen, Z. Chen, B. Chiaro, A. Dunsworth, A. G. Fowler, I.-C. Hoi, E. Jeffrey, A. Megrant, J. Mutus, C. Neill, P. J. J. O'Malley, C. Quintana, P. Roushan, D. Sank, A. Vainsencher, J. Wenner, T. C. White, A. N. Cleland, and J. M. Martinis, Phys. Rev. Lett. **112**, 240504 (2014).

[9] D. J. Egger and F. K. Wilhelm, Phys. Rev. Lett. **112**, 240503 (2014).

[10] S. Machnes, E. Assémat, D. Tannor, and F. K. Wilhelm, Phys. Rev. Lett. **120**, 150401 (2018).

[11] M. Devoret and R. J. Schoelkopf, Science **339**, 1169 (2013).

[12] D. J. Egger and F. K. Wilhelm, Supercond. Sci. Technol. **27**, 014001 (2014).

[13] R. Schutjens, F. A. Dagga, D. J. Egger, and F. K. Wilhelm, Phys. Rev. A **88**, 052330 (2013).

[14] P. J. Liebermann, P.-L. Dallaire-Demers, and F. K. Wilhelm, arXiv:1701.07870.

[15] R. W. Heeres, P. Reinhold, N. Ofek, L. Frunzio, L. Jiang, M. H. Devoret, and R. J. Schoelkopf, Nat. Commun. **8**, 94 (2017).

[16] M. H. Goerz, F. Motzoi, K. B. Whaley, and C. P. Koch, npj Quantum Inf. **3**, 37 (2017).

[17] P. Marquetand and V. Engel, J. Chem. Phys. **127**, 084115 (2007).

[18] V. Engel, C. Meier, and D. J. Tannor, Local control theory: Recent applications to energy and particle transfer processes in molecules, in *Advances in Chemical Physics* (John Wiley and Sons, Inc., Hoboken, NJ, 2009), Vol. 141, pp. 29–101.

[19] B. F. E. Curchod, T. J. Penfold, U. Rothlisberger, and I. Tavernelli, ChemPhysChem **16**, 2127 (2015).

[20] R. Kosloff, A. D. Hammerich, and D. Tannor, Phys. Rev. Lett. **69**, 2172 (1992).

[21] B. F. E. Curchod, T. J. Penfold, U. Rothlisberger, and I. Tavernelli, Phys. Rev. A **84**, 042507 (2011).

[22] D. C. McKay, S. Filipp, A. Mezzacapo, E. Magesan, J. M. Chow, and J. M. Gambetta, Phys. Rev. Appl. **6**, 064007 (2016).

[23] M. Roth, M. Ganzhorn, N. Moll, S. Filipp, G. Salis, and S. Schmidt, Phys. Rev. A **96**, 062323 (2017).

[24] J. Koch, T. M. Yu, J. Gambetta, A. A. Houck, D. I. Schuster, J. Majer, A. Blais, M. H. Devoret, S. M. Girvin, and R. J. Schoelkopf, Phys. Rev. A **76**, 042319 (2007).

[25] S. B. Singh and C. A. Singh, Am. J. Phys. **57**, 894 (1989).

[26] J. A. Nelder and R. Mead, Comput. J. **7**, 308 (1965).

[27] N. Moll, P. Barkoutsos, L. S. Bishop, J. M. Chow, A. Cross, D. J. Egger, S. Filipp, A. Fuhrer, J. M. Gambetta, M. Ganzhorn, A. Kandala, A. Mezzacapo, P. Müller, W. Riess, G. Salis, J. Smolin, I. Tavernelli, and K. Temme, Quantum Sci. Technol. **3**, 030503 (2018).

[28] D. J. Egger, G. Ganzhorn, Marc amd Salis, A. Fuhrer, P. Mueller, P. K. Barkoutsos, N. Moll, I. Tavernelli, and S. Filipp, Phys. Rev. Appl. **11**, 014017 (2019).

[29] P. K. Barkoutsos, J. Gontier, I. Sokolov, N. Moll, G. Salis, A. Fuhrer, M. Ganzhorn, D. Egger, M. Troyer, A. Mezzacapo, S. Filipp, and I. Tavernelli, Phys. Rev. A **98**, 022322 (2018).

[30] D. Kraft, *A Software Package for Sequential Quadratic Programming*, Deutsche Forschungs- und Versuchsanstalt für Luft- und Raumfahrt (DFVLR, Köln, 1988).

[31] M. Mariantoni, H. Wang, R. C. Bialczak, M. Lenander, E. Lucero, M. Neeley, A. D. O'Connell, D. Sank, M. Weides, J. Wenner, T. Yamamoto, Y. Yin, J. Zhao, J. M. Martinis, and A. N. Cleland, Nat. Phys. **7**, 287 (2011).